Incorporating of Lawsonia inermis as a bio-template for synthesising of NiO

nanoparticles: a potential antibacterial agent

Abbas Bagheri Khatibani ¹, Mohammad Hadi Ahmadi ¹

¹Department of Physics, La.C., Islamic Azad University, Lahijan, Iran

Abstract

This work details the synthesis of NiO nanoparticles, one of the most abundant metal oxides,

under varying conditions. A green hydrothermal route utilizing Lawsonia inermis (henna) as a

bio-template was employed. By adjusting the hydrothermal temperature from 140 °C to 180 °C,

three distinct samples (Ni-140, Ni-160, and Ni-180) were produced. The XRD patterns showed

excellent agreement with the standard NiO phase. Based on the XRD data, the structural

parameters of NiO samples have been analyzed, too. Morphological analysis via FESEM

indicated discrete nanoparticles for Ni-140 and Ni-180, whereas the Ni-160 sample was

agglomerated. Optically, the transmittance at 550 nm was measured at 62%, 46%, and 47%,

leading to band gap energies of 3.78 eV, 3.82 eV, and 3.90 eV, respectively. These band gap

values are consistent with previously reported data. According to calculations, the crystallite size

for all samples was about 14 nm. The efficacy of metallic oxide nanoparticles as antibacterial

agents is attributed to their innate nanoscale dimensions and their increased capacity for

interaction with biological structures.

Keywords: Lawsonia inermis, green hydrothermal, NiO nanoparticles, physical study

1

1. Introduction

Plant extracts play a versatile role in nanoparticle synthesis by functioning as combined reducing, capping, and stabilizing agents. The mechanism involves the organization and entrapment of metal ions within molecular structures like amylose helices, while plant surfaces provide a biotemplate that regulates size and inhibits agglomeration [Bulla et al., 2024]. The superiority of plant-based synthesis lies in its operational simplicity, economic viability, and environmental safety [Khashaei et al., 2022]. This is attributed to the high concentration of phytochemicals, which are capable of controlling nanoparticle formation [Etefa et al., 2023]. Although various biological templates—from animal skeletons to bacteria—are available, plantbased routes are notably more resource-efficient and less costly [Mohandesi et al., 2022]. Key biomolecules featuring amino, hydroxyl, and carboxyl groups, as well as alkaloids and flavonoids, are responsible for reducing metal ions and stabilizing the resultant nanoparticles [Khashaei et al., 2022]. Lawsonia inermis (henna), rich in phytochemicals, exemplifies this principle. Its primary bioactive component, lawsone (2-hydroxy-1,4-naphthoquinone), is accompanied by a diverse profile of secondary metabolites including coumarins, flavonoids, and tannins, all contributing to its efficacy in nanoparticle synthesis [Lazim et al., 2025].

The domain of green synthesis is focused on establishing environmentally benign and sustainable methodologies through the reduction or elimination of hazardous solvents. This paradigm aligns with the principles of green chemistry, facilitating the production of low-cost, stable, and reproducible nanomaterials [Khashaei et al., 2022]. It utilizes renewable biological resources, including plant extracts, enzymes, and microorganisms, as precursor materials. A pervasive issue in nanomaterial fabrication is particle aggregation, which compromises functional surface area. The application of capping agents is a critical strategy to inhibit this aggregation and regulate

morphological development. While traditional surfactants and polymers are common, there is growing interest in natural alternatives derived from a vast array of biological sources such as seeds, fruit peels, and biopolymers. These natural agents present a safer, eco-friendly advantage over their synthetic counterparts, which are associated with potential health and environmental risks due to the release of carcinogenic substances [Al-Yunus et al., 2024].

Metal oxides are extensively researched for their natural abundance and environmentally benign nature. In nanoparticle form, they exhibit high surface areas and exceptional chemical and thermal stability [Moradnia et al., 2024]. Among them, nickel oxide (NiO) NPs are particularly noteworthy, distinguished by their straightforward synthesis, cost-effectiveness, and safe handling [Gunasekaran et al., 2021]. Structurally, NiO is an antiferromagnetic p-type semiconductor; its charge transport, which occurs predominantly through holes, is influenced by the presence of Ni³⁺ and Ni²⁺ ions in the lattice [Bulla et al., 2024]. The material's considerable scientific appeal stems from its adjustable band gap (typically 2.3–4.0 eV), high thermochemical stability, low toxicity, and minimal environmental impact [Istrate et al., 2025]. Consequently, NiO nanoparticles demonstrate remarkable versatility, finding utility in diverse fields including energy storage (batteries, solar cells), sensing (gas sensors), smart materials (electrochromic devices, smart windows), photocatalysis, and biomedicine as cytotoxic agents [Khashaei et al., 2022; Moradnia et al., 2024; Gobinath et al., 2023]. Besides a diversity of bacteria, including both Gram-positive and Gram-negative species, NiO nanoparticles have potential antibacterial action. Even though, their dimensions to produce reactive oxygen species (ROS) play a role in the demise and damage of bacterial cells. There are numerous reports of the use of the NiO NPs as an antibacterial agent (Gebretinsae et al., 2019; Iqbal et al., 2019; Din et al., 2018; Sukumaran et al., 2025).

The present study was designed to develop a novel green synthesis route for NiO nanoparticles, utilizing a byproduct of henna leaf extract as a multifunctional bio-agent for reduction and stabilization. The process is facilitated by key phytochemical constituents in the extract, notably lawsone (2-hydroxy-1,4-naphthoquinone) and gallic acid, which are instrumental in the reduction of metal ions and ensuring nanoparticle stability [El-Fitiany et al., 2025]. This work, to the best of our knowledge, represents the first instance of employing henna extract in a hydrothermal method for NiO nanoparticle fabrication. The synthesis was conducted by varying the hydrothermal temperature, and the resulting samples were thoroughly examined to determine their physical characteristics.

2. Preparation of NiO nanoparticles (NPs)

Fresh henna leaves were thoroughly rinsed with distilled water to remove surface impurities. Subsequently, 10 grams of the cleaned leaves were chopped into fine pieces and mechanically ground using a blender. The ground plant material was then heated in 100 mL of purified water at 70 °C for one hour. The resulting mixture was filtered to obtain a clear extract, which was further purified by centrifugation at 2000 rpm for 10 minutes. The final filtrate was used immediately for nanoparticle synthesis. In a typical synthesis, 25 mL of the freshly prepared henna extract was added to 40 mL of a 0.1 M nickel nitrate (Ni(NO₃)₂) solution. The mixture was vigorously stirred on a magnetic stirrer at a temperature between 60-70 °C for 30 minutes. The homogeneous solution was then transferred into a 100 mL Teflon-lined stainless-steel autoclave and subjected to hydrothermal treatment at three different temperatures: 140 °C, 160 °C, and 180 °C, for duration of 18 hours. After the autoclave cooled naturally to room temperature, the resulting precipitate was collected and dried in an oven at 700 °C for 1.5 hours.

This procedure was repeated consistently to synthesize all samples (denoted as Ni-140, Ni-160, and Ni-180 based on their respective hydrothermal temperatures).

3. RESULTS AND DISCUSSION

3.1. Morphological study

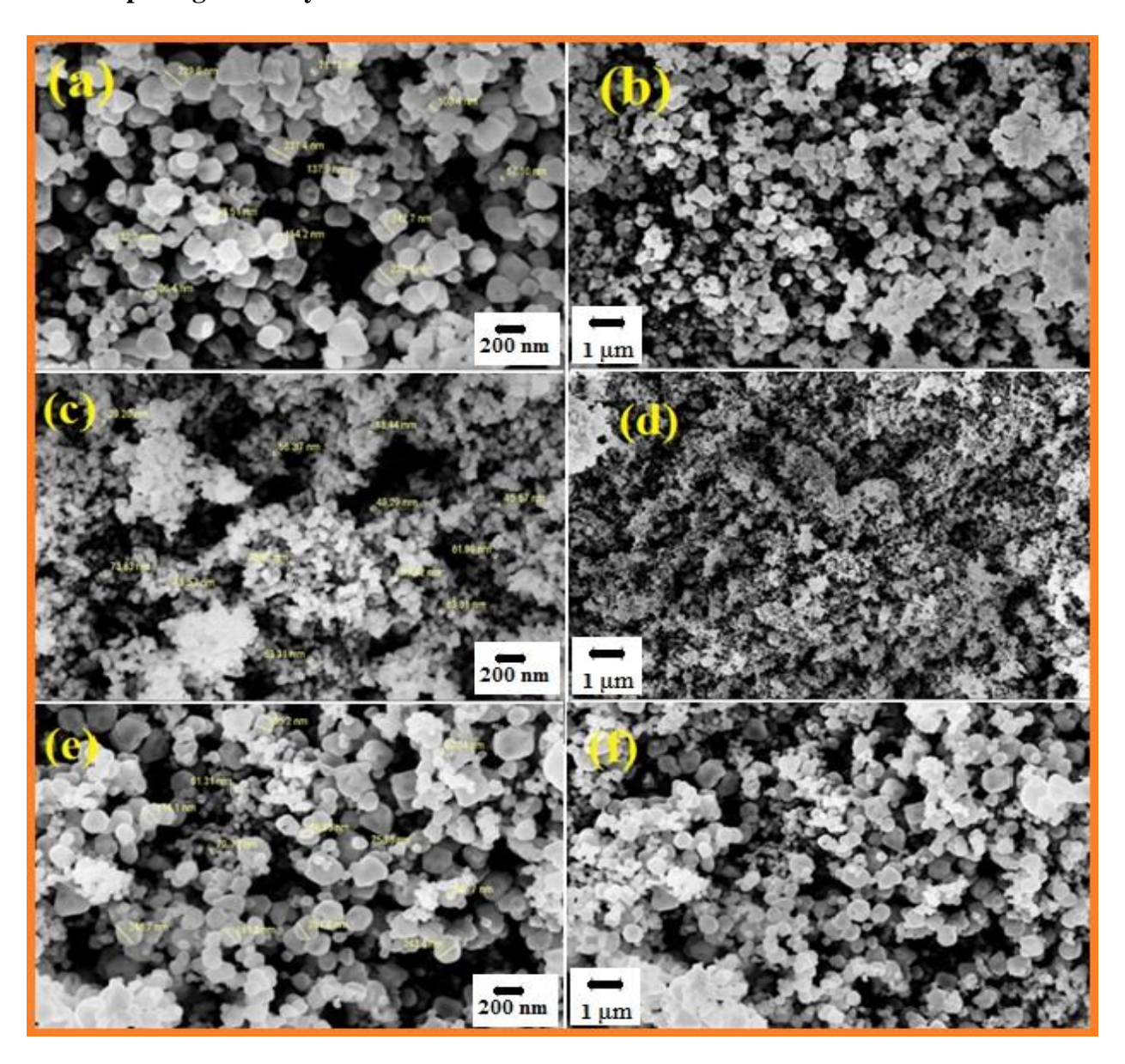


Fig. 1. FE-SEM images NiO synthesized at 140°C (a, b), 160°C (c, d) and 180°C (e, f) hydrothermal temperature.

FE-SEM images in Figure 1, exhibit NiO morphology synthesized at 140, 160 and 180°C. The figures demonstrate the morphological variation with temperature at (140, 160 and 180°C). The influence of temperature appears to be a critical factor in determining the morphology, particle size and distribution of synthesized NiO. As observing all the images, we find the regular distribution of the particles, but the separation of the particles can be seen at a temperature of (140) with an irregular shape and with different diameters ranging between 57.1 to 242.7 nm (figure (1 (a,b))), and this manner was repeated at the temperature of 180°C too. But with different diameters ranging from 61.31 - 248.7 nm in the figure (1 (e,f)), whereas looking at the figure (1 (c,d)) at the temperature of 160°C, we find that the particles are agglomerated with diameters ranging from 38.67 to 73.63 nm.

As it is clear, the yield of NiO NPs at 140 and 180°C are the more homogeneous and separated suggesting that effective surface area should be more observable at Ni-140 and Ni-180.

3.2 Structural study

Phase identification and crystallinity of the synthesized nanoparticles were assessed using X-ray diffraction (XRD). As illustrated in Figure 2, the diffraction patterns for all samples match the reference for standard polycrystalline cubic NiO (space group Fm-3m, JCPDS card No. 01-078-0643). The absence of extraneous peaks confirms the high phase purity of the products. The primary reflections, corresponding to the (111), (200), (220), (311), and (222) lattice planes, are consistently present. A key observation is the enhanced relative intensity of these peaks in the Ni-160 sample, which suggests a higher degree of crystallinity achieved at this specific synthesis temperature.

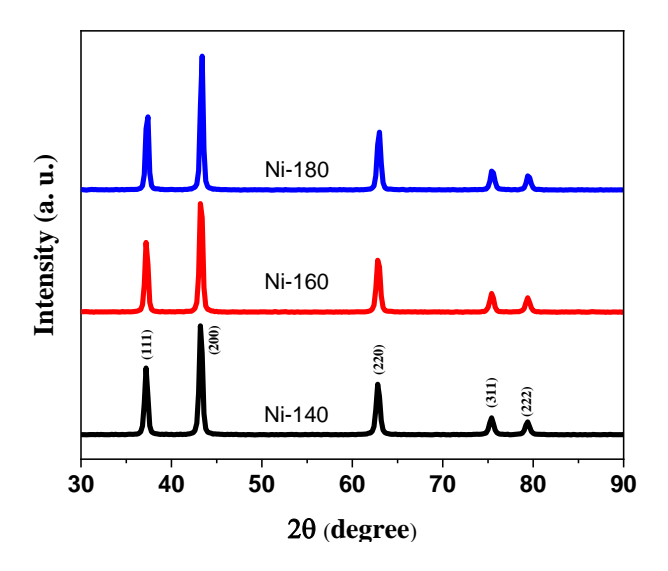


Fig.2. The XRD graph of nickel oxide based samples

Table 1. The structural lattice parameters calculated with the (200) diffraction peak.

Sample	$d = (\stackrel{\circ}{A})$	a = b(A)	Volume	
	Cal. Sta.	Cal. Sta.	of unit cell $(\stackrel{\circ}{A})^3$	
			Cal. Sta.	
Ni-140	2.092 2.088	4.184 4.176	73.238 72.830	
Ni-160	2.091 2.088	4.182 4.176	73.139 72.830	
Ni-180	2.087 2.088	4.175 4.176	72.751 72.830	

For the most intense XRD peak, the lattice constants were calculated and compared with the standard values (Table 1). Variations were observed due to differences in preparation conditions. While all samples show values close to the standard, Ni-180 exhibits the closest match. Minor deviations from the standard are present, likely arising from lattice strain and instability. It is well known that various structural defects can influence the band edge variation process.

Based on the XRD data, the structural parameters of NiO samples have been analyzed. The crystallite size and specific surface area were determined using the following methods:

$$D = \frac{0.9\lambda}{\beta \cos \theta} \tag{1}$$

$$S = \frac{6}{D \times \rho} \tag{2}$$

$$\delta = \frac{1}{D^2} \tag{3}$$

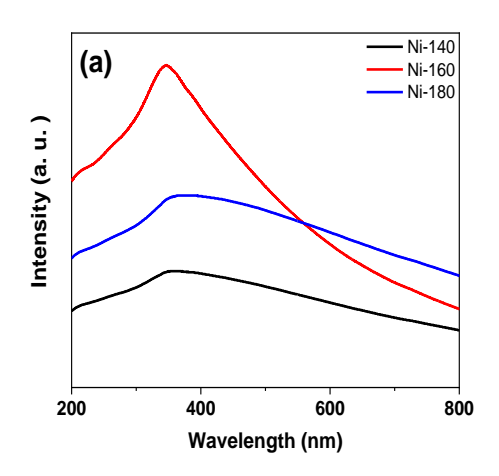
$$SF = \frac{2\pi^2}{45(3\tan\theta)^{\frac{1}{2}}}\beta$$
 (4)

Where λ is the X-ray wavelength used, β is the full width at half-maximum, θ is the Bragg's angle and ρ is the related density. These factors were estimated and listed in Table 2. It is noteworthy that the crystallite size increased slightly with the rise in hydrothermal temperature, by approximately 2.6%. This variation in crystallite size can be imputed to bond length contraction and expansion, bond angle variations, twisting, twinning, and interstitial defects in the lattice structure [Saadat Niavol et al., 2023]. As the crystallite size increases, specific surface area, and dislocation density decrease. The highest value of specific surface area and dislocation density belongs to Ni-140.

Table 2. Various parameters of the zinc manganite structure.

Sample	D(nm)	$S \times 10^3 (\frac{m^2}{Kg})$	dislocation density	stacking fault (SF)	Density
		$\frac{3 \times 10}{Kg}$	$\times 10^{-6} (nm^{-2})$	×10 ⁻⁶	(g/mol)
Ni-140	13.547	65.394	5449	2419	6.773
Ni-160	13.644	64.841	5372	2764	6.782
Ni-180	13.904	63.293	5173	1723	6.818

3.3 Optical Study



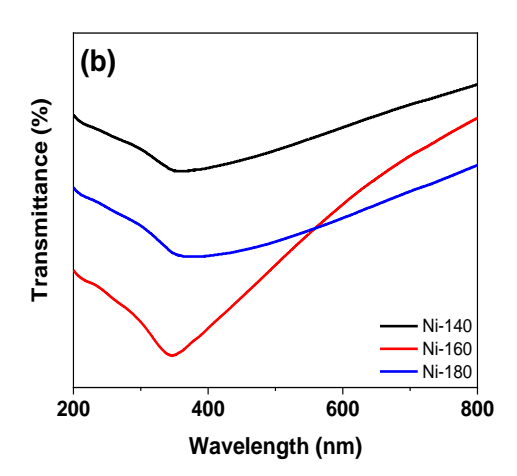


Fig. 3. Absorbance (a) and transmittance percentage (b) of green synthesized NiO samples.

UV-Vis spectroscopy was employed to investigate the optical behavior of the synthesized NiO nanoparticles, a critical property for semiconductor materials. The absorbance spectra (Figure 3) for all samples show a characteristic rise near 350-360 nm, corresponding to the fundamental absorption edge where electrons are excited from the valence band to the conduction band [Saadat Niavol et al., 2024]. A slight shift in this absorption edge is observable between samples. Furthermore, analysis of the transmittance spectra reveals significant differences, with Ni-140 exhibiting the highest transmittance (62%) at 550 nm, compared to 46% for Ni-160 and 47% for Ni-180. These disparities in optical transmission can be correlated to morphological characteristics, such as variations in particle size, agglomeration, and surface morphology, which affect light scattering [Bagheri Khatibani et al., 2015; Khoshhal et al., 2024]. Exclusively, according to Mie theory, smaller nanoparticles primarily absorb light, while larger nanoparticles increasingly scatter it. A higher-temperature synthesis producing larger particles will therefore

show increased scattering at longer wavelengths, raising the baseline absorption (and reducing transmission) in the UV-Vis-NIR spectrum.

To determine the optical band gap of all samples, the Tauc equation has been used:

$$\alpha h \nu = A \big(h \nu - E_g \big)^n \tag{5}$$

Where α is absorption coefficient, h denotes Planck's constant, ν denotes the frequency of light, A denotes the absorption constant, $h\nu$ denotes the energy of a photon and E_g denotes the energy of the band gap. Depending on the type of transition, n takes on a variety of values, including 2 for an indirect authorized transition, 1/2 for a direct allowed transition. It is possible to get a decent approximation of E_g in eV unit from the intercept of the tangent of the curve of $(\alpha h v)^{1/n}$ versus hv. The Tauc method was employed to quantify the optical band gap, with the exponent nn set to 1/2, corresponding to a direct allowed transition characteristic of NiO. The derived band gap energies were 3.61 eV, 3.71 eV, and 3.57 eV, respectively (figure 4). These band gaps are close to the declared values for NiO by Sathish Kumar et al. [Sathish Kumar et al., 2017]. The systematic variation in E_{g} across the samples can be attributed to differences in their microstructural characteristics. It is well-established that the electronic structure, and consequently the band gap, is highly sensitive to factors such as lattice strain, grain size (quantum effects), and the density of defects [Karouei et al., 2024; Beigli et al., 2023]. The observed trend suggests that the synthesis conditions directly influenced these microstructural parameters.

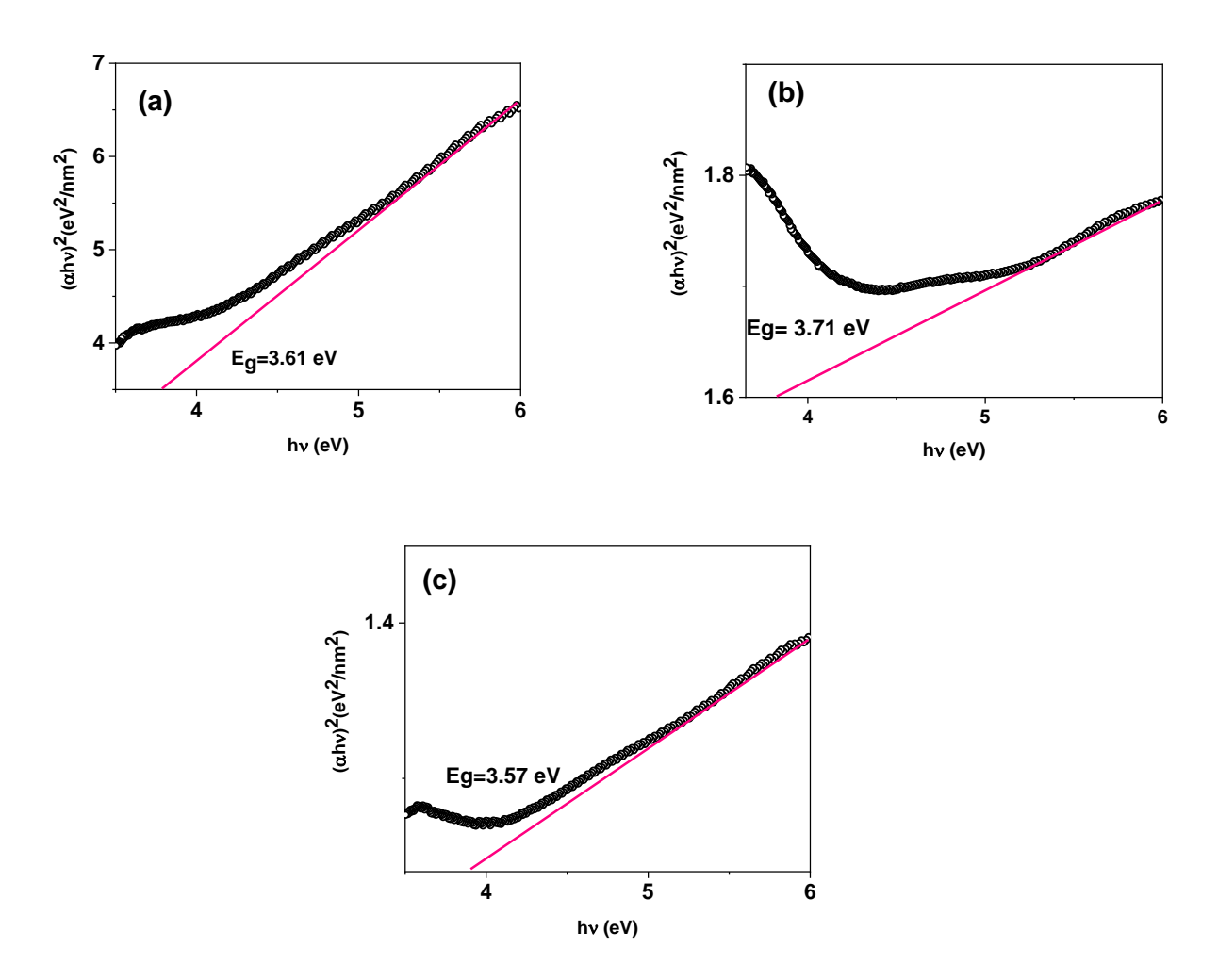


Fig. 4. optical bandgap of green synthesized NiO (a) Ni-140 (b) Ni-160 and (c) Ni-180.

4. Conclusion

The potential of metallic oxide nanoparticles as antibacterial tools is linked to their inherent nano-size and enhanced ability to interact with biological entities. This work demonstrates the successful green synthesis of nickel oxide (NiO) nanostructures using Lawsonia inermis (henna) extract as a bio-capping agent under hydrothermal conditions (140–180 °C). The structural and optical characterization confirmed the high quality of the products. XRD patterns indicated a pure NiO phase without impurities, and FESEM analysis established the nanoscale morphology

of all samples. Furthermore, UV-Vis spectroscopy showed that the samples exhibited tunable optical properties, with transmittance at 550 nm ranging from 46% to 62% and direct band gaps between 3.78 and 3.90 eV, in good agreement with reported values. These findings confirm the efficacy of the green synthesis route and lay the groundwork for future biological studies.

6. References

Al-Yunus A., Al-Arjan W., Traboulsi H., Schuarca R., Chando P., Hosein I.D., Hessien M. (2024). Effect of Synthesis Conditions on CuO-NiO Nanocomposites Synthesized via Saponin-Green/Microwave Assisted-Hydrothermal Method. Nanomaterials, 14, 308.

Bagheri Khatibani, A., Abbasi, M. (2015). Comparison of gas sensing properties of spray pyrolysed VOx thin films, Journal of Materials Science: Materials in Electronics, 26, 5052.

Beigli H., Shaddoust M., Ahmadi M.H., Bagheri Khatibani A. (2023). Effect of low and relatively long-term gamma irradiation on physical properties of ZnO and ZnO: Co thin films, Journal of Sol-Gel Science and Technology, 108, 798.

Bulla M., Kumar V., Devi, Kumar R.S., Sisodiya A.K., Dahiya R., Mishra A.K. (2024). Natural resource-derived NiO nanoparticles via aloe vera for high-performance symmetric supercapacitor, Scientific Reports, 14, 7389.

Din M. I., Nabi A. G., Rani A., Aihetasham A., Mukhtar M. (2018). Single Step Green Synthesis of Stable Nickel and Nickel Oxide Nanoparticles From Calotropis gigantea: Catalytic and Antimicrobial Potentials, Environmental Nanotechnology, Monitoring & Management 9, 29. El-Fitiany R.A., El Nahas R., Al Balkhi S., Aljaeedi S., Alblooshi A., Hassan F.M., Khaleel A., Samadi A., Khasawneh M.A. (2025). Alchemy in Nature: The Role of Lawsonia inermis Extract

Choice in Crafting Potent Anticancer Metal Nanoparticles, ACS Applied Materials & Interfaces, 17, 3, 4637.

Etefa H.F., Nemera D.J., Dejene F.B. (2023). Green Synthesis of Nickel Oxide NPs Incorporating Carbon Dots for Antimicrobial Activities, ACS Omega 8 (41), 38418.

Gebretinsae H. G., Tsegay M. G., Nuru Z. Y. (2019). Biosynthesis of Nickel Oxide (NiO) Nanoparticles From Cactus Plant Extract, Materials Today: Proceedings, 36, 566.

Gobinath E., Dhatchinamoorthy M., Saran P., Vishnu D., Indumathy R., Kalaiarasi G. (2023). Synthesis and characterization of NiO nanoparticles using Sesbania grandiflora flower to evaluate cytotoxicity, Results in Chemistry, 6, 101043.

Gunasekaran S.S., Gopalakrishnan A., Subashchandrabose R., Badhulika S. (2021). Phytogenic generation of NiO nanoparticles as green-electrode material for high performance asymmetric supercapacitor applications. Journal of Energy Storage 37, 102412.

Iqbal J., Abbasi B. A., Mahmood T., Hameed S., Munir A., Kanwal S. (2019). Green Synthesis and Characterizations of Nickel Oxide Nanoparticles Using Leaf Extract of Rhamnus virgata and Their Potential Biological Applications, Applied Organometallic Chemistry, 33, e4950.

Istrate D., Oproescu M., Modan E.M., Moga S.G., Negrea D.A., Schiopu A.G. (2025). Nanoscale Nickel Oxide: Synthesis, Characterization, and Impact on Antibacterial Activity Against Representative Microorganisms. ChemEngineering, 9, 77.

Karouei, S.F.H., Shaddoust, M., Khatibani, A.B., Rezapour A., Ahmadi M.H. (2024). Prominent ethylene glycol sensing of sol–gel-derived ZnO and Cu-ZnO nanostructures, Journal of Sol-Gel Science and Technology, 111, 736.

Khashaei M., Kafi-Ahmadi L., Khademinia S., Marjani A.P., Nozad E. (2022). A facile hydrothermal synthesis of high-efficient NiO nanocatalyst for preparation of 3,4-dihydropyrimidin-2(1H)-ones. Scientific Reports, 12, 8585.

Khoshhal A.R., Bagheri Khatibani A., Tirehdast Z., Shaddoust M., Nirouei M. (2024). Evaluation of experimental and simulated gamma ray shielding ability of ZnCo2O4 and ZnCo2O4/graphene nanoparticles, Optical Materials, 156, 115953.

Lazim K.A., Moghaddam H. M. (2025). Green Synthesis of Nickel Nanoparticles Using Lawsonia inermis Extract and Evaluation of Their Effectiveness against Staphylococcus aureus, Al-Mustansiriyah Journal of Science 36(1), 84.

Mohandesi M., Tavakolian M., Rahimpour M.R. (2022). Eggplant as an appreciable bio-template for green synthesis of NiO nanoparticles: Study of physical and photocatalytic properties, Ceramics International, 48(16), 22820.

Moradnia F., Taghavi Fardood S., Zarei A., Heidarzadeh S., Ramazani A., Sillanpaa M. (2024). Green synthesis of nickel oxide nanoparticles using plant extracts: an overview of their antibacterial, catalytic, and photocatalytic efficiency in the degradation of organic pollutants, Iranian Journal of Catalysis (IJC), 14(1), 142401 (1-24).

Saadat Niavol S., Bagheri Khatibani A., Imani S., Milani Moghaddam H. (2023). Ethylene glycol-sensing properties of hydrothermally grown feather-like ZnO nanopowder with abundant oxygen vacancies, Journal of Materials Research, 38, 1211.

Saadat Niavol S., Bagheri Khatibani A., Milani Moghaddam H., Gao G. (2024). ZnO quantum dots decorated on graphene oxide and graphene nanoplatelets: Comparison the structure and sensing properties, Inorganic Chemistry Communications, 160 111957.

Sukumaran J., Priya M., Venkatesan R., Sathiasivan K., Rashid Khan M. Kim S.C. (2025). Green Synthesis of Nickel Oxide Nanoparticles Using Leaf Extract of Aegle marmelos and Their Antibacterial, Anti-Oxidant, and In Vitro Cytotoxicity Activity, Microscopy Research and Technique, 88, 2830.

Sathish Kumar R., Johnson Jeyakumar S., Jothibas, Kartharinal Punithavathy M. I., Prince Richard J. (2017). Influence of molar concentration on structural, optical and magnetic properties of NiO nanoparticles, Journal of Materials Science: Materials in Electronics, 28, 15668.